System Identification and Control of an Aerobot Drive System

Paul Pounds [1], Robert Mahony [2], Peter Corke [3]
[12]*Department of Engineering, Australian National University*
Bld 32 North Road, Acton ACT 0200 Australia,
paul.pounds@anu.edu.au, robert.mahony@anu.edu.au
[3]*ICT Robotics, CSIRO*
1 Technology Court, Pullenvale QLD 4069 Australia, peter.corke@csiro.au

Abstract

Fast thrust changes are important for authoritive control of VTOL micro air vehicles. Fixed-pitch rotors that alter thrust by varying rotor speed require high-bandwidth control systems to provide adequate performace. We develop a feedback compensator for a brushless hobby motor driving a custom rotor suitable for UAVs. The system plant is identified using step excitation experiments. The aerodynamic operating conditions of these rotors are unusual and so experiments are performed to characterise expected load disturbances. The plant and load models lead to a proportional controller design capable of significantly decreasing rise-time and propagation of disturbances, subject to bus voltage constraints.

1. INTRODUCTION

Dynamic control is critical to unmanned aerial vehicle (UAV) flight. Craft that rely on changing rotor thrusts for manoeuvering, such as small tandems, quad-rotors or blimps, are a subset of UAVs for which rotor speed control is of great interest. These micro air vehicles use fixed-pitch rotors that vary thrust by changing angular velocity. Such designs avoid the complex swashplate mechanisms of fully articuled blades and so offer savings in complexity and maintenance. The robust simplicity of this style of rotor is one of the key driving motivations for the development of quad-rotor UAVs.

Fast response of the drive system is essential for attitude control of UAVs equipped with fixed-pitch rotors. These drive units must either have low rotor mass or use a control system to artificially improve performance. The popular RCtoys Draganflyer toy [2] uses light, simple rotors; most current quad-rotors use RCtoys components. The Draganflyer does not directly sense or control the rotor speed, but rather closes the loop around the motors and attitude via pitch and roll rate feedback. Larger quad-rotor UAVs, such as the Australian National University's (ANU) X-4 Flyer [8], have rotors with much more inertia than Draganflyer rotors. These need some schema to improve the bandwidth of the rotor response for attitude control to be robust.

Small-scale rotors in quad-rotor craft present a set of aerodynamic conditions that are unusual among aircraft. Identifying likely disturbances resulting from the operation of the rotors allows for the frequency response of the closed loop system to be tuned to reject unwanted variations in rotor speed. Transient environmental influences, such as gusts or wash from obstacles, are likely to be encountered by quad-rotor aircraft designed to operate in indoor spaces. Elimination of rotor speed deviations is desirable as this reduces the propagation of disturbances into the attitude dynamics of the vehicle. As yet, the influence of in-flight disturbances on small-scale rotor speed has not yet been explored.

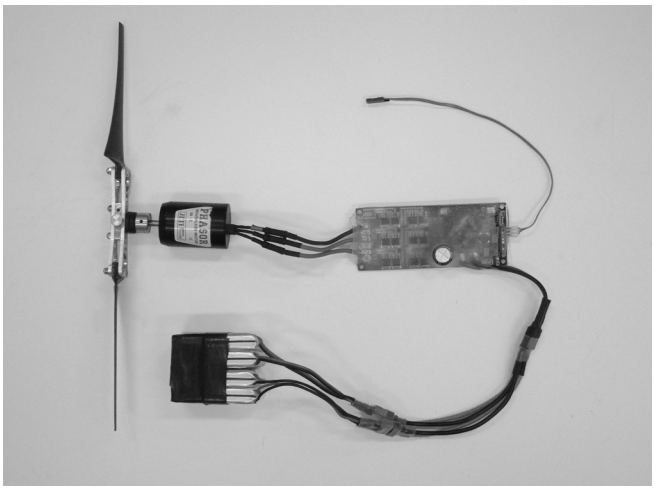

Fig. 1: Complete VTOL Thruster.

The controller for the small scale rotor drives we have developed (cf. Fig. 1) must improve the system bandwidth sufficiently for authorative attitude control on a quad-rotor vehicle. Rather than rely on empirial tuning or more complex nonlinear treatments, a rigorously designed controller based on a combined system model of the plant, verified by experiment, is warranted.

The compensator must be well-conditioned when used with a craft of loosely known and often changing flight parameters. The design must not exceed the limitations of the hardware in which it is implemented. Non-linearities of the system present bounds on the controller performance that must be respected. The controller is intentionally simple and practical to improve

1-4244-0902-0/07/$20.00 © 2007 IEEE

Authorized licensed use limited to: Linkoping Universitetsbibliotek. Downloaded on January 28, 2010 at 07:39 from IEEE Xplore. Restrictions apply.

the reliability of the system.

There are well developed theories for the control of fan speed driven by electric motors. Cogdel [1] and Innovatia [5] give comprehensive overviews of the dynamics of brushless motors, and Franklin and Powell [3] provide examples of motor control. Although more complex control methods exist, they are not appropriate technology to a system motivated by simplicity.

This paper is a case-study in the development of feedback control compensator for regulating rotor speed and improving bandwidth of an integrated drive control system for a small vertical take-off and landing (VTOL) aircraft. We outline the performance specifications of a custom rotor, motor and power system. We test the rotors for dynamic response and identify a model of the system plant and disturbances. We describe the process used to develop performance requirements and the logic behind the compensator design. Finally, we present the measured performance of the implemented controller.

2. HARDWARE

Each drive system consists of four components: rotors, motors, control boards and batteries, described below.

- Rotor
  The rotor is superficially similar to hobby aeroplane propellers. Unlike airscrews, the rotors must be matched to static thrust conditions. This makes the rotor blades thin and flexible with a flapping hinge, rather than chunky with high pitch angles [9].
- Motor
  Jeti Phasor 30-3 three-phase brushless motors for radio-controlled aircraft were selected for their high torque performance that allows for direct drive of the rotors, eliminating the need for gearing. The motors can pass more than 300 W and are rated up to 35 A.
- Controller Board
  Brushless motors require electronic commutation. RC hobby controllers are unsuitable due to non-linearities and bandwidth limitations. Custom control boards were made by the CSIRO ICT Queensland Centre for Advanced Technology group, based around the Freescale HC12D60A microprocessor and Toshiba TB9060 brushless motor speed controller .
  The boards also include an integrator single-phase back-emf speed sensor, as well as voltage and current sensors. The resolution of the speed sensor is limited by the rotation rate of the rotor and the number of magnetic poles. The maximum speed measurement refresh rate is 400 Hz and the current and voltage refresh rates are 50 Hz.
- Power
  Power is supplied by 32 Kokam lithium ion 1500 mAh high-discharge cells. Each cell has a nominal voltage of 3.7 V, ranging from 4.2 V fully charged and dropping to 3 V at depletion. Each cell can deliver 12 A constantly, or 15 A for short bursts. The batteries are connected in two parallel sets of four cells in series; that is, 14.8 V nominal voltage and 24 A of current.

3. ROTOR PERFORMANCE

Momentum theory provides a relationship between thrust, induced velocity and power in the rotor [10, pp6-7]. Using energy conservation, it can be shown that in hover:

$$P_i = \frac{T^{\frac{3}{2}}}{\sqrt{2\rho A}} \tag{1}$$

where T is the thrust produced, ρ is air density, A is the area of the rotor disc and P_i is the power induced in the air.

The Figure of Merit ($F.M.$) of the rotor is the ratio of power induced in the air and power in the rotor shaft:

$$F.M. = \frac{P_i}{P_s} \tag{2}$$

This is used to model rotor efficiency when calculating the theoretical onboard power requirements.

For a quad-rotor helicopter weighing 4 kg with a 30 per cent control margin, each motor must produce 12.7 N of thrust. The rotor radius is limited to less than 0.165 m, due to the size of the robot, leading to a requirement of 101.2 W of power induced in the air. The rotational velocity was set to 800 rads^{-1}. The lithium ion cells have a current limit of 22 A, producing a maximum 0.1749 Nm motor torque. This gives the drive a top shaft power of 131 W. The maximum theoretical thrust is 15.1 N per motor (assuming $F.M. = 1$). The actual rotor design $F.M.$ must be no less than 0.77.

In practice, the blades created were capable of producing 14.3 N at approximately 1000 rads^{-1}, a $F.M.$ of 0.71, but with a higher rotor speed.

4. DYNAMIC MODEL IDENTIFICATION

Fast dynamic response of rotor speed is essential for effective performance. Controlling the motors via a feedback compensator is a simple way to extract better rise-time. To design a controller, an accurate characterisation of the system is necessary. This is found using a set of step response experiments to identify the open loop plant of X-4's motor-rotor system previously described.

A. Dynamic Model Structure and Nonlinearities

The dynamic model of the rotor-motor system is composed of a cascade of the rotor aerodynamics, motor dynamics and battery response.

- Rotor Aerodynamics
  The rotor torque is modelled as a constant gain at operating conditions. The step response of the rotors is also expected to be very fast. Leishmann provides a quantitative estimate of the timescale of unsteady flow [6, pp369-371]. We found the flow rise-time of these rotors to be of the order of one blade revolution (less than 8 ms). This is very fast compared to the plant mechanics and so is not included in the model.

Authorized licensed use limited to: Linkoping Universitetsbibliotek. Downloaded on January 28, 2010 at 07:39 from IEEE Xplore. Restrictions apply.

- Motor Poles
  From Cogdell [1, p805], the dynamics of an ideal brushless motor system is given to be a two-pole system. One pole is associated with the rigid body dynamics of the motor and the other with the electrical dynamics of the windings. The mechanical pole is governed by the rotational inertia of the drive – the combined total of the rotating motor armature, blades, hub and mast. The electrical dynamic of brushless motors is typically very fast and is omitted.
- Battery Model
  Based on the theory and example cell parameters given in Gao *et al* [4], the flyer batteries are expected to have a one-pole, one-zero system model. No explicit identification of the battery dynamics has been performed. From previous experiments, it is known that the cells do not have a constant voltage during discharge. The voltage per cell drops substantially during the first and last 100 mAh of discharge. The mid-zone of operation is a gently decreasing slope. The rate of the battery voltage change is slow and we do not believe it will substantially affect the dynamics of the system.

The total cascaded system model is expected to take the form of two poles and one zero:

$$H = \frac{k(s + z_b)}{(s + p_m)(s + p_b)} \tag{3}$$

Where H is the plant model, k is the rotor gain, z_b is the battery zero and p_m and p_b are the motor and battery poles.

B. Step Response Experiments

The thruster step response was found using input excitation experiments. The data are used to identify the model parameters, based on the expected model stucture.

The step signal is a Pulse Width Modulated (PWM) signal sent to the motor control chip in a 255-step duty cycle, to modulate the pulse widths of voltage sent to the motor drive phases and drive the rotor. The drive components are mounted on the X-4 Flyer for the test. The flyer is fastened to a testbed that holds the robot off the ground and allows it to be locked in place or pivoted freely along the pitch axis.

The helicopter will predominately operate around hover, with a rotor speed of 850 rads^{-1}. The reference signals of 175-225 PWM units produce speeds of 820-920 rads^{-1}, respectively. This is a step across the full expected range of the rotor. The ID experiment was performed with a train of 70 step inputs, each with a period of 6 seconds.

A National Instruments 6024E DSP card captured the rotor's speed and input reference signal via a filtered frequency-to-voltage converter reading from one of the motor's three phases. The onboard speed measurement capabilities of the motor controller boards were not used for the identification as the data output of the sensor boards is limited to 50 Hz and is unsuitable for this purpose. The DSP measures a voltage produced by a speed sensor that reads the back-emf frequency of one of the motor phases. The sensor board has dynamics

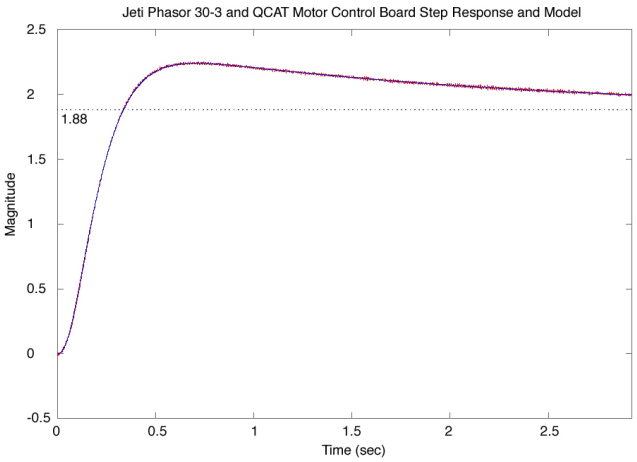

Fig. 2: Averaged Step Response Data of FH and Identified Model

associated with low-pass filters and a charge pump with slow electrical dynamics. The sensor board transfer function is:

$$F = \frac{442}{(s + 45)(s + 9.7)} \tag{4}$$

The DSP samples at 1 kHz and the speed sensor can resolve speed differences of 1.2 rads^{-1}.

All of the tests were averaged to increase the signal-to-noise ratio (SNR) of the data. The noise of the signal has a peak-to-peak magnitude of 10 rads^{-1}, for an SNR of 38 dB. Averaging the step responses increases the SNR to 57 dB. The model identified included a 0.02 second time delay in the system; this is attributed to the influence of fast dynamic effects and processor transport delay. The averaged measured response curve data of the combined plant and sensor dynamics, with the estimated sensor-plant model step response super-imposed, is shown in (cf. Fig. 2).

The plant transfer function is found by inverting the identified combined sensor-thruster system by the known sensor model. The identified thruster response was found to be:

$$H = \frac{23(s + 0.43)}{(s + 9.6)(s + 0.54)} \tag{5}$$

The pole-zero pair is attributed to the slow dynamics of the batteries, and one dominant pole to the mechanical response of the rotor. Although filtering the logged data with an inverted sensor model produced a noisy signal, the output had good agreement with the expected drive dynamics.

The step response and Bode plot of the plant appear in figures (cf. Fig. 3) and (cf. Fig. 4).

Associated with the lithium ion cells is a slew rate non-linearity. When the motor is given a large step instruction, the instantaneous current flow is large – in the order of 100 A. The internal resistance of the cells causes the terminal voltage of the battery to fall dramatically during high current draw. The motor control board is powered by a 5 V regulator across the input supply – if the battery voltage falls below this, the microprocessor loses power and resets. For this reason,

Authorized licensed use limited to: Linkoping Universitetsbibliotek. Downloaded on January 28, 2010 at 07:39 from IEEE Xplore. Restrictions apply.

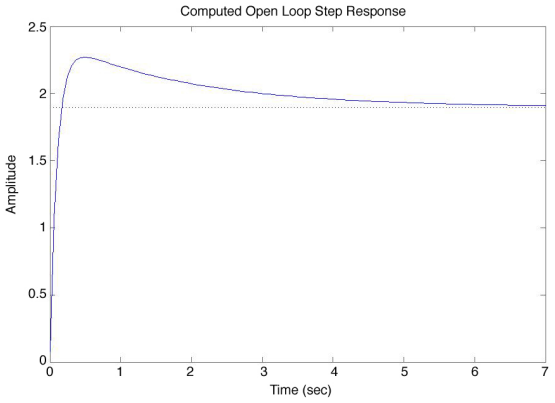

Fig. 3: Open Loop Plant Step Response

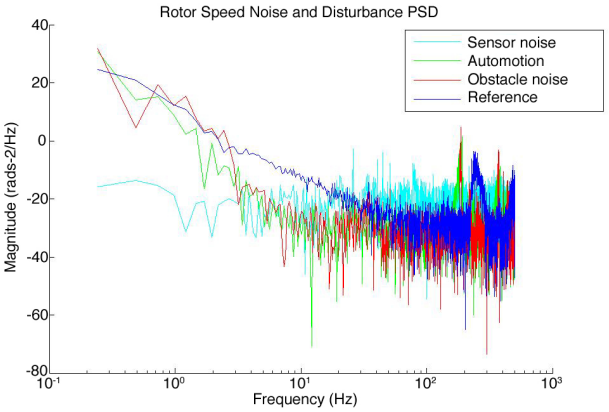

Fig. 5: Power Spectral Density of Noise and Disturbance Tests

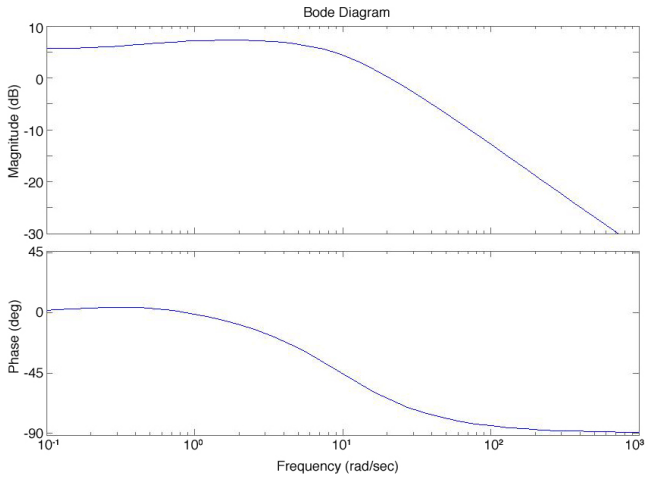

Fig. 4: Open Loop Plant Bode Plot

the controller must not make large increases, or series of increments, in motor demand that drive the voltage below the cutoff. Empirical tests show that constant increasing steps of up to 8 per cent of full throttle per time sample can be tolerated.

The maximum current draw of the cells is 12 A. At full throttle, the motor will spin up to a maximum speed of 1050 rads^{-1}. The motor electrical phase cannot be reversed during flight for dynamic braking.

5. Noise and Disturbance Model Identification

We know that the rotor thrust varies due to environmental effects such as turbulence and crosswinds. Uncontrolled variations in speed are passed as disturbances to the rigid-body dynamics of the helicopter. Desirably, a SSFP rotor system will be resilient to inputs of this type. As thrust cannot be directly measured easily, rotor speed is used as a metric instead.

By analysing variation in the rotor speed from a set of experiments replicating likely noise scenarios, the Power Spectral Density (PSD) distribution of typical disturbances can be determined. The PSD can then be mapped back into disturbances in the rotor thrust to provide a disturbance model for the rigid-body dynamics of the airframe. From this, a set of performance criteria can be made for use in designing a rotor compensator.

We used this data to develop a model of the speed disturbances encountered by the X-4 drive system on a test-bed. We catagorise the rotor disturbances into four types: environment effects, automotion effects, obstacle effects and sensor noise. Environmental effects are due to the dynamic behaviour of the surrounding atmosphere – breezes, updrafts and eddies. Automotion effects are due to the helicopter's motion in the air. Obstacle effects are caused by proximity to objects and surfaces. Sensor noise is random level fluctuation in the measured speed values.

Four tests were performed:

- Environment effects test – constant PWM, static position
- Automotion effects test – constant PWM, flyer rocked back and forth by hand
- Obstacle effects test – constant PWM, static position, a large flat surface moved around the rotor
- Sensor noise test – motor stopped, sensor values recorded

In each test, the rotor speed was sampled at 1 kHz with the National Instruments card and Matlab Realtime Windows. Approximately 70 seconds of data was recorded each time.

The PSD of each signal indicates what frequencies are present (cf. Fig. 5). The tests show a body of low frequencies (< 100 rad^{-1}) associated with the dynamic disturbances. The sensor noise test produced a flat spectrum of noise. The noise floor of the signals is found to be approximately -30 dB.

Each test exhibited a set of frequency spikes between 150 and 300 rads^{-1} associated with noise from a nearby power supply. Frequencies higher than 300 rads^{-1} are attenuated by the dynamics of the motor. Changing battery voltage levels introduced very low frequencies into the spectrum.

A 600-second-long environment test was performed to improve low-frequency spectrum resolution. It exhibited the same low-frequency power distribution as the other environment test; all of the effects tests produced a similar frequency spectrum, with variations in power. When the PSD is plotted on a log-log graph it shows a linear trend (cf. Fig. 5).

Authorized licensed use limited to: Linkoping Universitetsbibliotek. Downloaded on January 28, 2010 at 07:39 from IEEE Xplore. Restrictions apply.

It is interesting to note that the undisturbed test has the greatest levels of higher-frequency noise. It is thought that this is due to circulating currents and eddies building up over time in a sustained flow. If the flow conditions are constantly disturbed, such systems cannot manifest. As a consequence, stable hover conditions correspond to the worse noise characteristics for the system.

6. CONTROL

The rotor speed controller must primarily provide stable and robust performance and disturbance rejection, as well as satisfy the constraints of the system limitations. Foremost is the slew rate; the controller implemention cannot exceed the slew rate bound imposed to avoid critical voltage drops. Disturbance rejection is also considered, as well as high frequency noise and the effect of limit-cycles.

A. Requirements and Constraints

The rate limitation of the system sets an upper bound on the gain and frequency of the input to the plant.

A maximum constraint for the realisable frequency response of the system can be can be developed by considering the fastest sinewave that the rate limitation can support. The highest frequency that can be passed through the rate saturation can be determined by equating the ramp magnitude to the maximum slope of the sinewave at a given frequency. The constraint is given as Ratelimit $= B$ units/s.

For a sinewave:

$$u = A\sin(\omega t) \tag{6}$$

$$\frac{du}{dt} = A\omega\cos(\omega t) \tag{7}$$

where A is the amplitude of the sinewave, t is time and u is the system input. The maximum slope is at $cos(\omega t) = 1$:

$$A\omega \leq B \tag{8}$$

Thus, A can be replaced with the magnitude of the input to the motor system. The largest step passed to the system will occur when the error is at the greatest expected value, Δ_e. In the closed loop case, with controller C and plant H, the bound (eq. 10) is derived as follows:

$$\Delta_e\|C\|\omega \leq B \tag{9}$$

$$\|C\|\|H\|\omega \leq \frac{B\|H\|}{\Delta_e} \tag{10}$$

$$20\log(\|C\|\|H\|) + 20\log(\omega) \leq 20\log(\frac{B\|H\|}{\Delta_e}) \tag{11}$$

$$20\log(\|C\|\|H\|) \leq 20\log(\frac{B}{\Delta_e}) \tag{12}$$
$$+20\log(\|H\|) - 20\log(\omega)$$

This is a limit on the open-loop compensated Bode plot, a function of ω. The rate saturation on the system is $B = 10$ pwm steps/ms. From the motor load disturbance tests, the greatest tolerated is set to be 5 rads^{-1}. The corresponding rate bound appears on the Bode plot in (cf. Fig. 6).

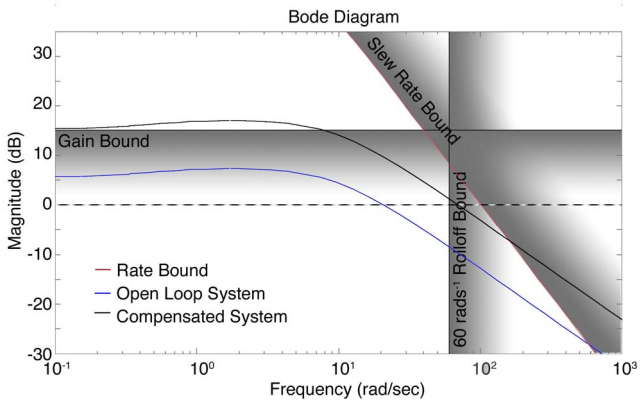

Fig. 6: System Design Constraints: Compensated System Magnitude Bode Plot (black) With Open Loop System (blue) and Rate Bound (red).

For disturbance rejection, we identify low and high frequency disturbances. The bulk of the disturbance spectral power is at low end of the spectrum, in particular at frequencies less than 30 rads^{-1}, with the power decaying up to 80 rads^{-1}. We seek to reduce the effect of the disturbances with two approaches. Firstly, the controller must attenuate peak disturbance power region introducing sufficent compensator gain at low frequencies. Secondly, the system must have sufficent bandwidth to attenuate signals up to the highest disturbance frequency.

The sensitivity function of the controller is:

$$S = \frac{1}{1 + \|C\|\|H\|} \tag{13}$$

We aim for -15 dB gain for attenuation of disturbance inputs. Further attenuation reduces the disturbance signal below what can be resolved by the speed sensor. It is known that $\|H\| = 1.8$ at low frequencies. Solving for $\|C\|$ gives a lower gain bound of $+8$ dB.

From S it can be seen that the stopband of the disturbances will be the passband of the closed loop system. Thus, to attenuate all disturbance frequencies, the closed loop plant must have a bandwidth of 80 rads^{-1}. We consider attenuation of only 60 rads^{-1} acceptable, as the remainder contains little power.

Reference tracking of the plant is not a consideration of the controller. It is expected that differences in speed will feed into the angular displacement of the helicopter. Disturbance rejection will be incorporated into the attitude controller and corrections will feed back into the speed control reference. Tracking a precise speed control is unnecessary for attitude control and this prevents multiple integrators from fighting each other in the integrated flyer system.

B. Compensator Design

The compensator chosen is a straight proportional controller. As the plant consists of a single dominant pole and a near

Authorized licensed use limited to: Linkoping Universitetsbibliotek. Downloaded on January 28, 2010 at 07:39 from IEEE Xplore. Restrictions apply.

pole-zero cancellation, the plant cannot be sent unstable by the application of gain. However, especially large values ($K > 5$) will introduce limit-cycles in the plant, caused by saturating the amplitude and slew rate bounds of the controller. We choose a value of 3, such that the response is made as fast as possible within the specified bounds.

From the model of the plant and non-linearities, we coded a simulation of the rotor dynamics in Matlab Simulink. This was used to assess the proportional controller and ensure that the controller design did not produce limit-cycles oscillations. The maximum step of 820–920 rads^{-1} may just begin to saturate the actuator. As the rate limitation sets a maximum response speed, this will ensure that the rise time is minimised without pushing the motor beyond what the limitation allows for.

The gain selected slightly pushes the controller frequency response out of the rate limitation bound at 5 rads^{-1}. The effect is not very pronounced and, given the improvements in rise-time, is considered acceptable. From calculation, the minimum gain necessary to satisfy the low frequency disturbance rejection criterion is 2.57. The system gain satisfies the original -15 dB specification, reaching -16.12 dB.

The computed transfer function of the closed loop system is:

$$H_{cl} = \frac{68.85(s + 0.42)}{(s + 78.54)(s + 0.43)} \tag{14}$$

C. Performance

The control design was implemented on the CSIRO boards and tested in the X-4 thrust test rig. The control loop runs at 1 kHz on the microprocessor – a speed dictated by the need to smoothly generate the rate-limited ramp output of the controllers. All control computations were performed with signed long variables, with up to 20-bits computational precision available from the HC12 arithmetic logic unit.

We repeated the ID process for the closed loop plant to confirm that the controller performs as designed. The identification showed good agreement with the calculated system:

$$H_{cl} = \frac{83(s + 0.0046)}{(s + 99)(s + 0.0042)} \tag{15}$$

The implemented system has a rise-time of 0.05 seconds and no overshoot. Higher gains were tested on the controller, but we felt the resulting cyclic behaviour that developed was too undesirable. The implemented system has a 70 rads^{-1} bandwidth, satisfying the bandwidth requirement. The overall performance of the system was deemed acceptable. In subsequent tests on the X-4 Flyer platform, it was shown that the thrusters respond fast enough to stabilise the craft.

7. Conclusion

We have fully characterised the response of the rotor speed dynamics of the X-4 Flyer's drive system. Experiments determined the power spectral density of environmental disturbances which were used to set specifications for noise rejection. We have implemented a speed regulator with much faster response than the open-loop system. The rise-time was reduced from 0.2 seconds to 0.05 seconds. Disturbance frequencies up to 60 rads^{-1} can be rejected by the controller, although some noise up to 80 rads^{-1} is not attenuated. The thruster performace is adequate and has proven sufficient for its designed purpose.

References

[1] J. Cogdel, *Foundations of Electrical Engineering*, 2nd Ed. Upper Saddle River, New Jersey: Prentice Hall, 1999

[2] Draganfly Innovations. (2006, Jan.) Draganflyer V Ti Thermal Intelligence Gyro Stabilized Helicopter. [Online]. Available: http://www.rctoys.com/draganflyer5.php

[3] G. Franklin, J. Powell and A Emami-Naeini, *Feedback Control of Dynamic Systems*, Reading, Massachusetts, United States of America: Addison-Wesley Publishing Company,1994

[4] L. Gao, S. Liu and R. Dougal, "Dynamic Lithium-Ion Battery Model for System Simulation", *IEEE Transactions on Components and Packaging Technologies*, Vol. 25, No. 3, Sept. 2002.

[5] Innovatia Design Center. (2006, Jun.) Motor Theory. [Online]. Available: http://www.innovatia.com/Design_Center/Electronic_Design_for_Motor_Control_1.htm

[6] J. Leishman, *Principles of Helicopter Aerodynamics*, Cambridge, United Kingdom: Cambridge University Press, 2000

[7] P. Pounds, R. Mahony, P. Hynes and J. Roberts, "Design of a Four-Rotor Aerial Robot", in *In proceedings of Australasian Conference on Robotics and Automation*, Auckland, New Zealand, 2002

[8] P. Pounds, R. Mahony, J. Gresham, P. Corke and J. Roberts, "Towards Dynamically-Favourable Quad-Rotor Aerial Robots", in *In proceedings of Australasian Conference on Robotics and Automation*, Canberra, Australia, 2004

[9] P. Pounds and R. Mahony, "Small-Scale Aeroelastic Rotor Simulation, Design and Fabrication", in *In proceedings of Australasian Conference on Robotics and Automation*, Sydney, Australia, 2005

[10] J. Seddon, *Basic Helicopter Aerodynamics*, Osney Mead, Oxford: Blackwell Science, 1996

Authorized licensed use limited to: Linkoping Universitetsbibliotek. Downloaded on January 28, 2010 at 07:39 from IEEE Xplore. Restrictions apply.